J Mater Sci (2009) 44:620–631
DOI 10.1007/s10853-008-3078-z

Microscopy and microanalysis of inorganic polymer cements. 2: the gel binder

Redmond R. Lloyd · John L. Provis · Jannie S. J. van Deventer

Received: 9 July 2008 / Accepted: 21 October 2008 / Published online: 10 November 2008

Abstract By scanning electron microscopy and microanalysis of fly ash-based and mixed fly ash-slag inorganic polymer cement (i.e., "fly ash geopolymer") binders, a more detailed understanding of the gel structure and its formation mechanism have been developed. The binder is predominantly an aluminosilicate gel charge balanced by alkali metal cations, although it appears that calcium supplied by slag particles becomes relatively well dispersed throughout the gel. The gel itself is comprised of colloidal-sized, globular units closely bonded together at their surfaces. The microstructure of the binder resulting from hydroxide activation of fly ash is much less uniform than that which forms in a corresponding silicate-activated system; this can be rationalized in terms of a newly developed explanation for the differences in reaction mechanisms between these two systems. In hydroxide activation, the newly formed gel phase nucleates and grows outwards from the ash particle surfaces, whereas the high silica concentration in a silicate-activated system enables a more homogeneous gelation process to take place throughout the inter-particle volume.

Introduction

As was discussed in detail in Part 1 of this series of papers [1], electron microscopic examination of inorganic polymer cements (IPC, and including the class of aluminosilicate materials known as "geopolymers") is able to provide key insight into the mechanism of formation of the inorganic gel binder phase. As this gel is predominantly responsible for the strength development of IPC, the factors controlling both the rate of its development and the structures thus formed are critical in understanding and tailoring IPC performance and properties. IPC is synthesized by alkali or alkali silicate activation of industrial waste materials; fly ash from coal combustion and/or blast furnace slag, with dissolution of the solid precursors resulting in the release of small aluminate and silicate species, which then polymerize to form an inorganic gel [2, 3]. As IPC has been proposed and commercialized as an environmentally beneficial alternative to Portland cement in construction applications [4], the development of a detailed understanding of its synthesis mechanism will enable accurate control of setting and strength development rates, which are critical in the application of a new material in large-scale construction.

Examination of fly ash particle remnants in IPC by scanning electron microscopy (SEM) has provided important insight into the processes occurring during reaction [1]. The phase of primary importance in IPC, however, is the gel-phase reaction product. Relatively few authors have commented on the morphology of the reacted phase of IPC. The reason for this is not immediately apparent; it may be that the material generally appears featureless in the SEM at lower magnifications. As has been reported previously, the microstructure of fly ash-based IPC becomes progressively more reacted as the amount of alkali and silicate in the activating solution is increased, with strength increasing accordingly [5–8]. Electron microscopic analysis of the dominant gel phases in hydrated Portland cement has provided critical information regarding the chemistry and microstructure of these phases [9, 10], which has been used in the development of detailed chemical models to describe the gel formation process. It is intended that the results

R. R. Lloyd · J. L. Provis (✉) · J. S. J. van Deventer
Department of Chemical & Biomolecular Engineering, University of Melbourne, Melbourne, VIC 3010, Australia
e-mail: jprovis@unimelb.edu.au

presented here will be used in conjunction with data from other experimental techniques [8, 11–14] and from computational modeling [2, 15], to provide a more detailed conceptual understanding of the process of IPC formation.

In this article, analysis of the microstructures and elemental distributions formed in IPC is used to develop a new explanation for the observed differences between silicate-activated and hydroxide-activated IPC. This explanation builds in part from the initial work presented by Duxson et al. [16], which relates specifically to metakaolin-based geopolymers rather than fly ash-based IPC, but which still contains some points of relevance. The conceptual model of Fernández-Jiménez et al. [17] for hydroxide-activated fly ashes also provides a good deal of information that is of value in understanding that system. However, these models will be extended and new concepts developed here to provide a more accurate description of the key differences between the two modes of activation, without the need to refer to speculation regarding processes such as the possibility of syneresis in the reacting gels. This article will therefore provide a significant step forward in the understanding of IPC gel formation, building on data available in the literature as well as the results published here and in Part 1.

Experimental methods

Sample preparation and SEM were conducted following the procedures detailed in Part 1 [1]. Briefly, fly ash (GFA) from Gladstone power station, Queensland, Australia and ground granulated blast-furnace slag (GGBS) supplied by Independent Cement and Lime, Australia were blended by hand with activating solutions formulated by mixing commercial sodium silicate solutions (Grade N, PQ Australia) with sodium hydroxide solution (50 wt.%, Aldrich, Australia) and RO-grade deionized water, as necessary to meet the desired activator composition. The compositions of the ash and slag are given in Table 1. The fly ash used contains ~14% mullite, ~7% maghemite, and ~3% quartz; the GGBS is X-ray amorphous. Hydroxide activating solutions were formulated by the same procedure but without the addition of silicate solution. Samples were cured in sealed molds at 65 °C for 48 h for silicate-activated samples; 80 °C for 48 h for hydroxide-activated samples. Water/binder ratios were 0.325 for fly ash-based samples and 0.350 for ash/slag blends. Unless specifically noted otherwise, activator compositions are specified to be 7 wt.% Na_2O by mass of solid precursor (ash + slag), with silicate activators also containing 7 wt.% SiO_2 by mass of solids.

SEM characterization (imaging and microanalysis) of IPC samples was conducted using an FEI Nova NanoLab dual beam FIB/SEM with thermal field emission source. This microscope was fitted with secondary electron (SE) and backscattered electron (BSE) detectors as well as an EDAX Genesis X-ray spectrometer system, and was operated at an accelerating voltage of 5 kV for imaging and 5–10 kV for microanalysis, as discussed in detail previously [1, 8]. All images presented depict polished surfaces. Samples were polished with successively finer grades of diamond paste, with the final step using 0.25 μm diamond paste, and with care taken to avoid exposing the samples to water during the polishing procedure [1]. Samples were coated with a thin carbon layer to provide conductivity.

Transmission electron microscopy (TEM) was conducted using an FEI Tecnai F20 TEM with thermal field emission source, operated at 200 kV accelerating voltage. Samples were prepared by the 'lift-out' technique as described in detail by Lloyd [8].

Table 1 Oxide compositions of raw materials, in wt.%, from X-ray fluorescence analysis

	Fly ash	GGBS
Na_2O	0.28	0.26
MgO	1.35	6.02
Al_2O_3	27.84	13.18
SiO_2	45.46	32.88
P_2O_5	0.53	0.00
SO_3	0.21	3.50
K_2O	0.47	0.32
CaO	5.60	40.05
TiO_2	1.36	0.66
V_2O_5	0.00	0.03
MnO	0.19	0.40
Fe_2O_3	11.21	0.32
LOI	2.71	1.19

LOI loss on ignition at 1000 °C

Results and discussion

Gel morphology

Figure 1 shows the structure of the gel in fly ash-based IPC in backscattered electron (BSE) images. The gel consists of globular units ca. 100 nm in diameter. These must be bonded where they intersect for the gel to be rigid. The interstitial space is empty under vacuum in the SEM; this comprises the pore space of the gel, and is normally filled with fluid. The gel is clearly highly porous, although without the large pores typical of Portland cement pastes. As was observed in Part 1 [1], the unreacted ash particles are embedded in the binder, and show a range of degrees of bonding to the gel. Particles which are less tightly bonded

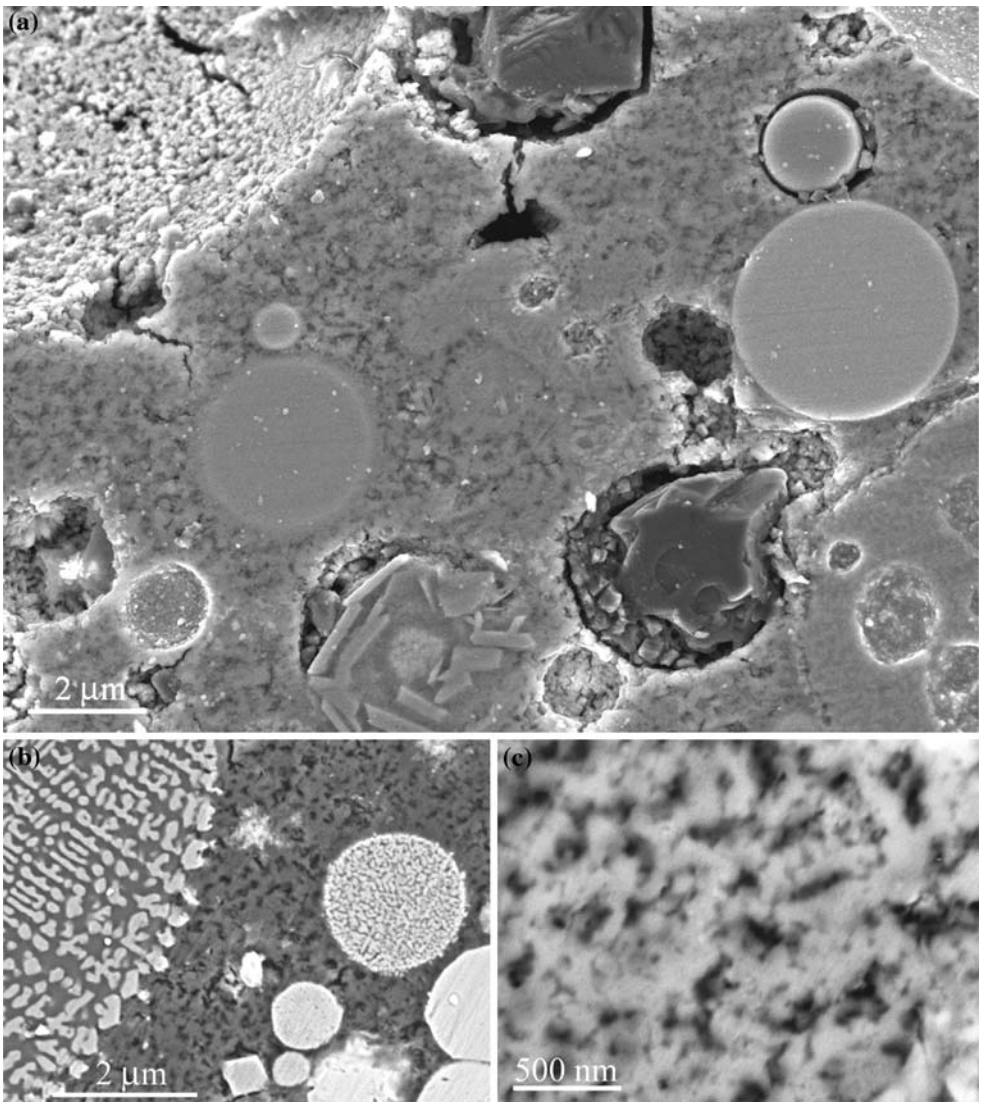

Fig. 1 BSE images of polished sections of silicate-activated fly ash IPC paste. **a** Section showing the porous nature of the gel and several embedded fly ash particles. **b** Section showing iron-rich particles of varying iron content (indicated by the relative brightness) surrounded by porous gel. **c** Magnified view of the structure of the gel. At high magnification, the resolution is degraded due to the electrons passing through the conductive carbon layer twice. Brightness was adjusted between images to allow for differences in composition, e.g., the iron-rich particles in (**b**)

to the gel are in general those which have continued to react after hardening of the IPC. The internal structures of some ash particles are also visible, while others appear featureless.

The pore structure is also clearly visible in TEM images, such as Fig. 2, and the importance of porosity in IPC has been discussed in detail by Lloyd [8]. Figure 2 shows significant similarity to the images presented by Sindhunata et al. [6]; it is additionally apparent from the images presented here that the structure of connected spheres extends evenly through the space between fly ash particles. Unlike the particles embedded within it, the gel appears evenly distributed with no apparent variation in gel density between the surface of ash particles and the bulk gel. This has important implications for the mechanism of gel formation, as will be discussed in depth later in this article. The gel structure observed has strong similarities to that observed when colloidal silica gels are prepared by destabilization of colloidal silica with potassium silicate solution [18].

The structure of the reaction product of alkali silicate-activated IPC appears very different from that of IPC activated with alkali hydroxide alone. Images of fly ash activated with 7 M NaOH and no dissolved silica are shown in Fig. 3; these are similar to those presented by Fernández-Jiménez et al. [19, 20] and Duxson et al. [3]. Contrary to the behavior of samples synthesized with alkali silicate-activating solutions (Fig. 1), the reaction products

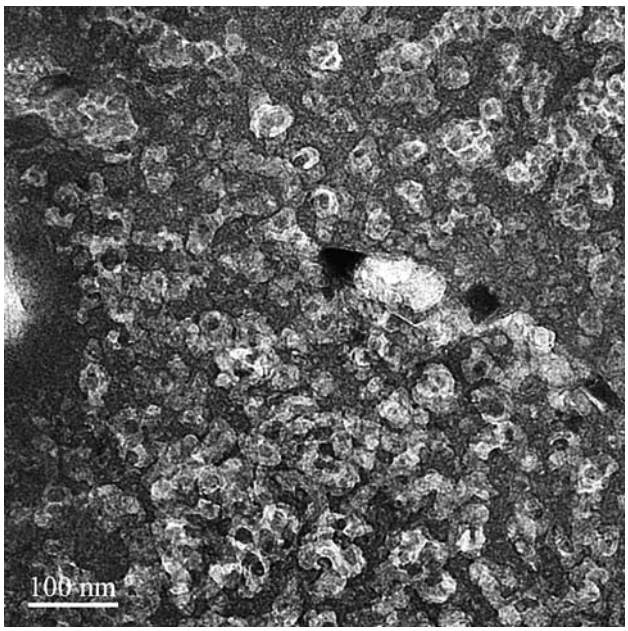

Fig. 2 TEM bright-field image of fly ash-based, silicate-activated IPC gel, showing the extensive porosity of the gel

in Fig. 3 appear to have formed preferentially on the surfaces of ash particles. The reaction products appear crystalline (zeolites were identified by X-ray diffraction) and granular, even at relatively low magnification in the SEM. Compared to alkali silicate-activated samples, relatively large voids exist within the structure.

The differences in microstructure of the gel help explain some characteristics of the performance of IPC. Criado et al. [21] observed the apparent paradox that silicate-activated IPC showed a lower extent of reaction but higher compressive strength than IPC activated with alkali hydroxide alone. While some of the difference could be accounted for by the silicate itself (i.e., for a given extent of ash dissolution, samples with soluble silicate added will have more available dissolved material than those without), it is highly likely that the differences in microstructure result in significantly different mechanical properties. The homogeneous distribution of the gel formed when dissolved silicate is present in the activating solution, along with the small size and high connectivity of the units making up the gel, would be expected to better distribute stress when the sample is under load. This would improve the compressive strength of the IPC. Conversely, the less homogeneous distribution of material in the silicate-free samples would result in higher local stress concentration under load and lower ultimate strength.

Implications for the mechanism of gel formation

The differences in structure between IPC activated with or without dissolved silica, as shown in Figs. 1 and 3, provide significant insight into the mechanisms of gel formation. When appreciable amounts of silicate are initially present in the activating solution (Fig. 1), three major differences in structure are apparent when compared with silicate-free samples (Fig. 3). First, the gel in the silicate-activated sample consists of very numerous and roughly similar-sized globular units; second, this gel appears the same throughout the sample, whether at the surface of the ash particles or relatively far away in the interstitial space; and third, no zeolites are observed, either by XRD or SEM. These differences imply significantly different pathways to structure formation, which can be explained well by reference to the solution chemistry of silica.

Because of its ability to polymerize, silica displays complex solution chemistry. It is generally accepted that the degree of polymerization of silicate species in the solution increases as silica concentration increases and as the ratio of silica to alkali hydroxide increases [22, 23]. Thus, at low silica concentrations or low silica to alkali ratio, the species present will be predominantly monomeric. At high concentrations and high ratios, higher-order species will predominate. This has been confirmed by Phair and van Deventer [24] and Duxson et al. [16] for the solutions used to activate IPC, using NMR spectroscopy, and was modeled by Provis et al. [25]. In isolation, aluminum displays less complex aqueous chemistry and is monomeric in the pH range of interest for IPC formation [26]. In the presence of dissolved silica, however, aluminum is able to substitute for silicon in many of the oligomeric anions that occur [26]. North and Swaddle [27] showed that the rate of exchange of silicate monomers with linear aluminosilicate species, i.e., $(OH)_3AlOSiO_n(OH)^{(n+1)-}_{(3-n)}$ with $n = 1$, 2, or 3, is much greater than with the analogous silicate dimers or with cyclic aluminosilicate species. This has consequences for solution-mediated processes. For instance, it was hypothesized that small linear aluminosilicate species add rapidly to growing zeolite crystals, rather than larger "kinetically inert" oligomers and cyclic structures which have traditionally been considered important for zeolite growth. This concept has gained widespread acceptance in zeolite chemistry [28–30].

From this discussion, it is apparent that the amount of dissolved silica present in the activating solution during IPC syntheses will control the speciation of silica and alumina which dissolve from the fly ash and thus influence microstructural development. Dissolution of silicon and aluminum into a solution with no initial silicate will result in small highly reactive species, i.e., $Al(OH)^-_4$ and $SiO_n(OH)^{n-}_{(4-n)}$ monomers and $(OH)_3AlOSiO_n(OH)^{(n+1)-}_{(3-n)}$ dimers. As well as exchanging with one another in the solution, these species are able to interact with the surface of fly ash particles and precipitate thereon. This was

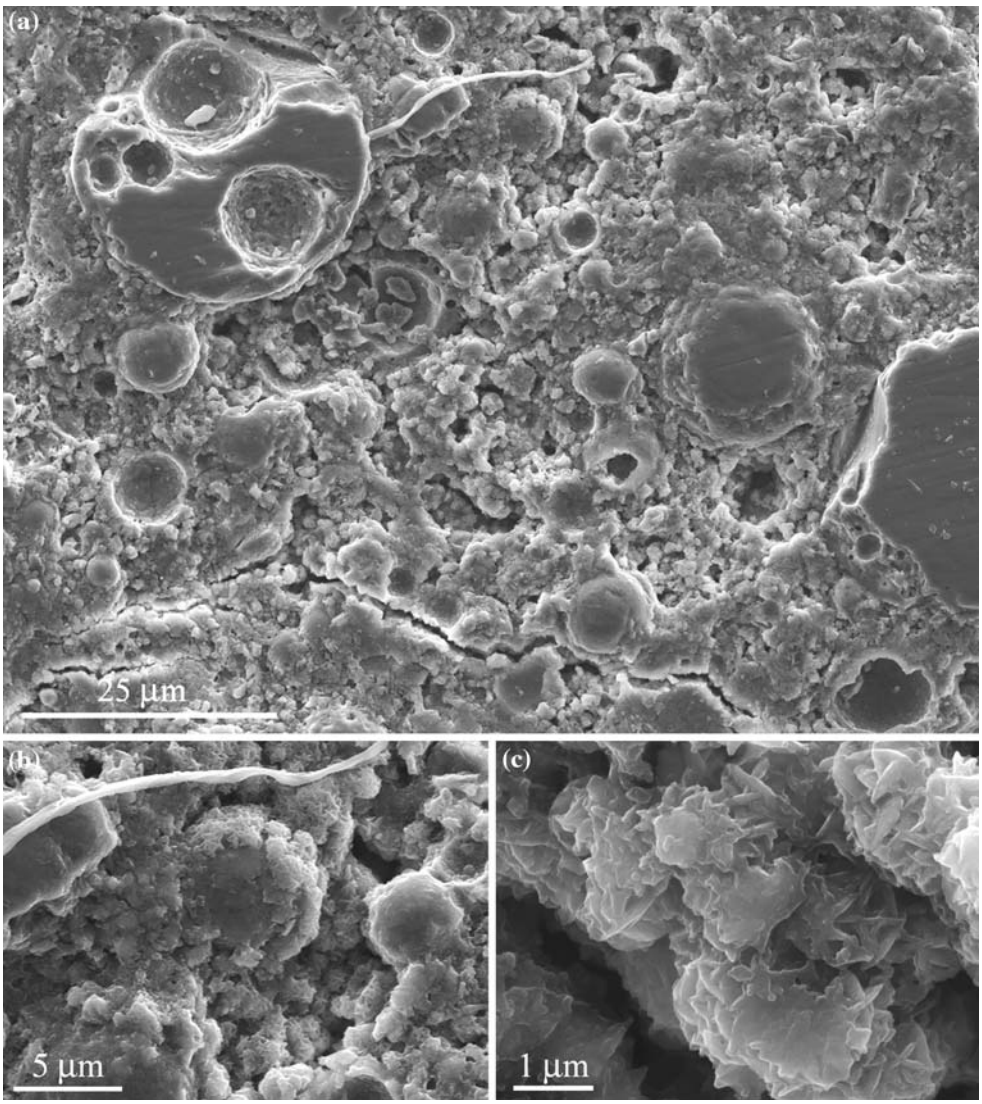

Fig. 3 **a** Secondary electron image of NaOH-activated fly ash paste. The sample was polished; however, the local structure was too weak to withstand the shear experienced during polishing and the sections are effectively fracture surfaces. **b** Reaction products form on the surface of fly ash particles. **c** The reaction products appear crystalline

demonstrated by the experiments of Lee and van Deventer [31] for fly ash-based IPC systems.

The mechanism proposed here for the microstructural development of hydroxide-activated IPCs is essentially consistent with the propositions of Fernández-Jiménez et al. [17], but provides more detail in a number of areas. Dissolution of the reactive phases in the ash and slag particles leads to the release of small silicate and aluminate species, in addition to other elements including calcium. As some of these small aluminosilicate small species precipitate back onto the fly ash particle surfaces, they may either redissolve or become fixed to the surface as further units condense over them. As more silica and alumina are provided into solution by glass dissolution, condensation back onto the surfaces of particles will result in the accretion of gel in these regions. Furthermore, the presence of aluminum in highly labile species will enhance zeolite nucleation; crystal growth will be able to occur as a result of the small, reactive species present in the solution [27].

As the thickness of the gel and zeolite layer increases it will grow outwards from the particle surfaces. Adjacent particles will eventually grow sufficiently close to bond at their points of contact, producing a solid mass with large interstitial voids. The microstructure observed in Fig. 3 is entirely consistent with this description: gel and zeolite crystals are observed on the surface of ash particles with void space in between, indicating growth outwards from the particle surface. One consequence of the layer of gel and zeolite growing on the surface of ash particles is that further dissolution of the underlying glass will be hindered; this is reflected in the greatly reduced early strength of IPC activated with hydroxide alone, compared to samples

activated with dissolved silicate present in the activating solution [21]. The possibility of tailoring nucleation behavior by the addition of nanoparticle seeds has been explored recently by Rees et al. [32]; while those authors did not publish strength data, they did observe significant differences in reaction rates as measured by in situ infrared spectroscopy. These data were explained in terms of nucleation on the seed surfaces altering the chemistry of the bulk gel formation, and so are also consistent with the observation of gel growth from ash particle surfaces as proposed here.

In contrast to the case of hydroxide activation is the case where fly ash is activated with alkaline solutions containing significant amounts of dissolved silica. In these systems, as silica and alumina are released from the glass surface into solution they may precipitate back onto the surface of the ash particle, as in hydroxide activation. However, the presence of high levels of dissolved silica means that they may also react with the species already present in the solution to form dimers or oligomers. In essence, there is competition for newly dissolved species between the fly ash surface and silicate species already in the solution. The enormous difference in number of reactive sites present in the solution, i.e., 4 for each monomer, 6 for each dimer, etc., versus the relatively small number of sites present on the surface of the ash particle will ensure that the overwhelming majority of dissolved silica and alumina will add to the species in the solution rather than condensing back onto the ash surface. This correlates with the observations of Lee and van Deventer [33] that there exists a threshold silicate concentration ($\sim$200 mM in their study) below which precipitation onto the particle surfaces impacted dissolution of fly ash into the alkaline solution. When a higher concentration of dissolved silicate was used by those authors, the species dissolving from the fly ash particle surfaces migrated away from the particles and into the bulk solution. The concentration of hydroxide, which controls the polymerization degree of silica, and the solid/liquid ratio of the system will both impact the exact threshold concentration, meaning that the 200 mM observed by Lee and van Deventer [33] is an indicative but not an universal value.

Continued addition of monomers to oligomeric aluminosilicate species will result in the growth of larger polymeric units of colloidal dimensions; further addition of material will result in gelation. The colloidal-sized units are clearly visible in the micrographs of alkali silicate-activated IPC shown in Fig. 1. Because of the relatively free movement and even distribution of material in the solution before gelation occurs, the microstructure formed is more homogeneous than for samples which set by growth outwards from the surface of ash particles, i.e., samples synthesized with low silicate-to-alkali ratio.

A consequence of the presence of larger oligomeric species in the solution will be reduced lability, and thus suppression of zeolite nucleation. The absence of detectable zeolites in alkali silicate-activated IPC is well known [21, 34], and is explained well by the hypothesis presented here.

The explanation developed here rationalizes the observed differences in microstructure and rates of strength gain of samples synthesized with or without silicate in the activating solution. As discussed earlier, the formation of a precipitate on the surface of fly ash activated without silicate would hinder further dissolution by providing a barrier to diffusion. Conversely, when silicate is present, sequestration of dissolving Si and Al in the growing species in the solution prevents the build up of a surface layer. Thus, silicate solutions activate the dissolution of fly ash more successfully than hydroxide alone, as observed previously [7, 31]. Once a gel has formed, however, convective transport is no longer possible and movement of species in the sample is greatly hindered, particularly considering the small pore sizes observed in silicate-activated samples. For samples activated without silicate, setting occurs by contact between the layers accreted on adjacent ash particles; this would have a relatively small effect on continued dissolution, as transport through the gel and zeolite layer on the particle surface would remain rate limiting. Thus, after setting, fly ash activated without dissolved silicate would react relatively faster than silicate-activated samples.

This hypothesis correlates well with the observations of Criado et al. [21] in their study of the compressive strength and extent of dissolution of fly ash activated with sodium hydroxide and varying levels of dissolved silica. For samples activated with high dissolved silica concentration, early strength was high with relatively modest increase thereafter. Conversely, samples activated with little or no dissolved silica showed poor early strength but a subsequent steady increase. The extent of activation, estimated from the remaining (unreacted) vitreous content of the ash, was higher for samples activated without silicate than those with hydroxide alone. This is likely because the first result reported was after 8 h curing at 85 °C; this is well after the onset of gelation, which could be expected after 30–45 min under such conditions. If the experiment was repeated and points obtained nearer to setting, it is likely that the extent of activation of silicate-activated samples would be higher than that of samples activated with hydroxide alone.

Elemental distributions in IPC

The distribution of elements in IPC is a significant aspect of the microstructure, particularly as phases may form that are not distinguishable by morphology alone. Maps of

elemental distributions were produced using SEM/EDX. Maps were obtained at three different magnifications to ensure that any sign of phase separation was not overlooked, either because it was at a scale too small to see, or larger than the area being examined. The accelerating voltage was varied from 10 to 5 kV as the magnification was increased, to reduce the interaction volume for X-ray generation as the pixel size decreased, as discussed previously [1]. Despite the low over-voltage for calcium K_α X-ray generation at 5 kV, sufficient signal to form useful maps was amassed by lengthening the beam dwell time per pixel and increasing the number of frames collected. Maps were obtained by summation of numerous frames, rather than slow collection of a single frame, to reduce specimen damage and migration of elements (particularly alkalis) which was observed to be significant with long beam dwell times. Elemental mapping was carried out on mixed fly ash/slag IPC samples rather than simply fly ash-based IPC, as the combination of the two precursors will provide useful information regarding more different elements and for elements supplied in a wider variety of chemical forms of importance in IPC synthesis.

Figure 4 shows an elemental map of aluminum within a mixed fly ash/slag IPC. It is apparent that the aluminum in IPC is strongly concentrated in residual fly ash particles. Heterogeneous distribution of aluminum within the ash particles can be seen particularly in high magnification images [8]. The brightness of GGBS grains is slightly higher than the surrounding gel, indicating that the aluminum content of the gel is similar to or slightly lower than that of GGBS. Within the gel itself, the distribution of aluminum appears to be homogeneous. At an accelerating voltage of 5 kV features smaller than 500 nm are clearly resolved, in accordance with the Monte Carlo simulations presented in Part 1 [1].

The distribution of silicon within a mixed fly ash/slag IPC, as shown in Fig. 5, is more homogeneous than that of aluminum. Regions of high concentration visible at low magnification (Fig. 5a) are probably quartz, which is invariably present in fly ash. At high magnification (Fig. 5b), depletion of silicon from the rims of the GGBS grains is apparent. The reasons for silicon depletion in these specific areas are not intuitively apparent from the chemistry of the binder-forming system, with a high silicate concentration in the activating solution not seeming to provide a strong driving force for silicon. However, an explanation for the observed behavior can be generated by consideration of the distribution of several of the other elements present, in particular magnesium, and will be elaborated below.

Figure 6 shows the distribution of sodium in IPC. Unlike silicon and aluminum, sodium appears unevenly distributed through the gel, and is concentrated around the

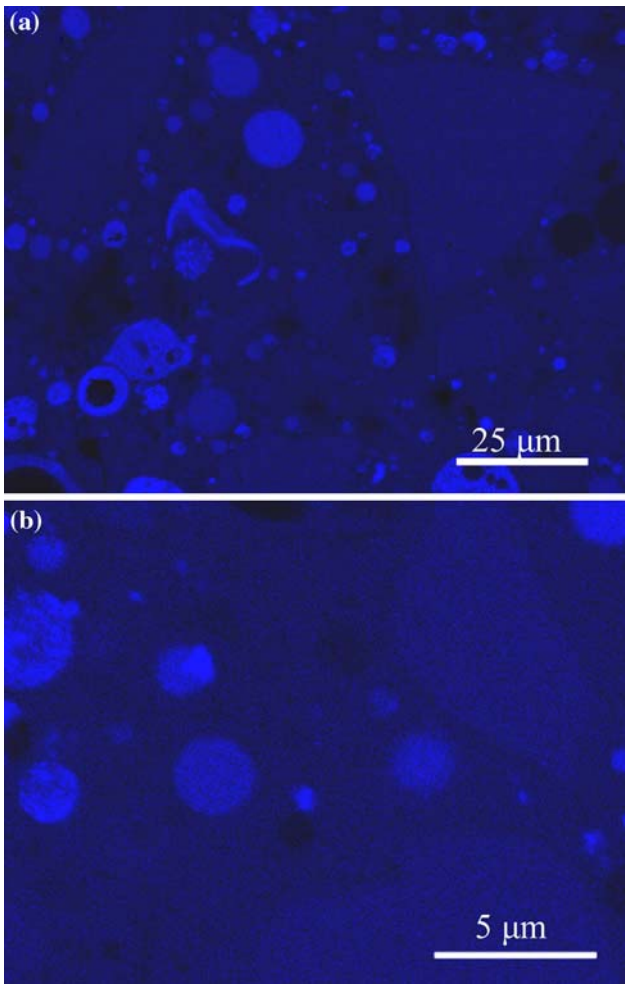

Fig. 4 Aluminum K_α X-ray maps for a blended GFA/GGBS (1:1) IPC activated with sodium silicate solution (7 wt.% Na_2O, 7 wt.% SiO_2 with respect to solid components)

rims of some particles—both ash and slag. This does not appear to be selective, and so is not likely to be strongly correlated to the silicon depletion noted above, which is only observed around slag grains. Increased sodium concentration in areas near particles may result from sodium in the pore solution becoming concentrated around the particle rims due to the increased local porosity left by the recession of dissolving glass, as was shown in Part 1 [1]. Rowles and O'Connor [35] and Blackford et al. [36] proposed that sodium is able to migrate within geopolymer samples when under electron irradiation in the TEM and SEM, respectively; this was minimized by the X-ray mapping procedure used here, however the effect may not have been eliminated entirely.

Figure 7 shows elemental maps of calcium in the same sample as is depicted in Figs. 4, 5, and 6. The distribution of calcium within the gel binder appears homogeneous on length scales from hundreds of micrometers to hundreds of nanometers (i.e., the resolution limit for Ca-K_α X-rays at an

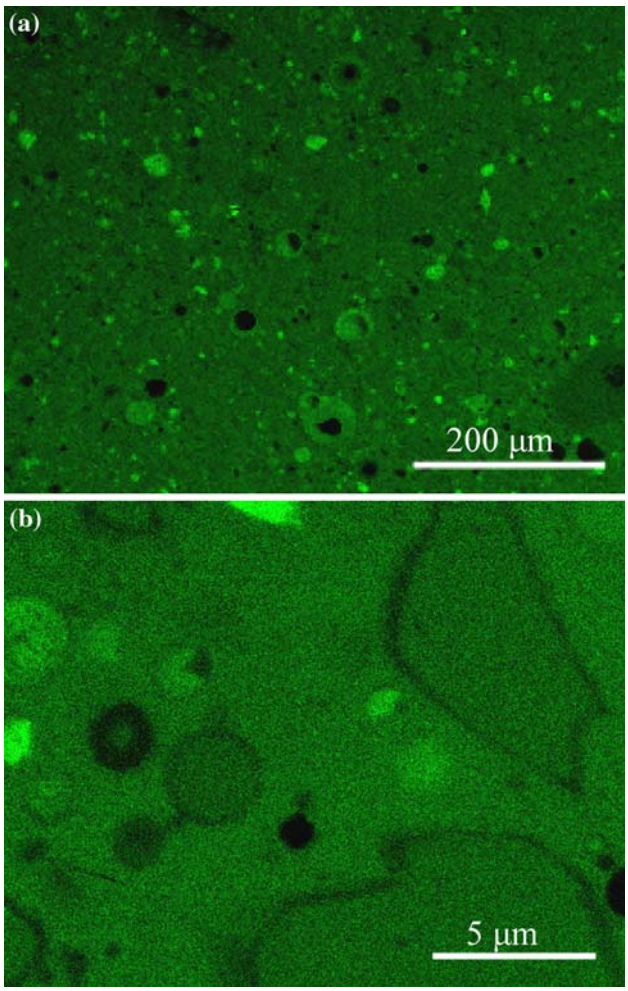

Fig. 5 Silicon K_α X-ray map for a blended GFA/GGBS (1:1) IPC activated with sodium silicate solution (7 wt.% Na_2O, 7 wt.% SiO_2 with respect to solid components)

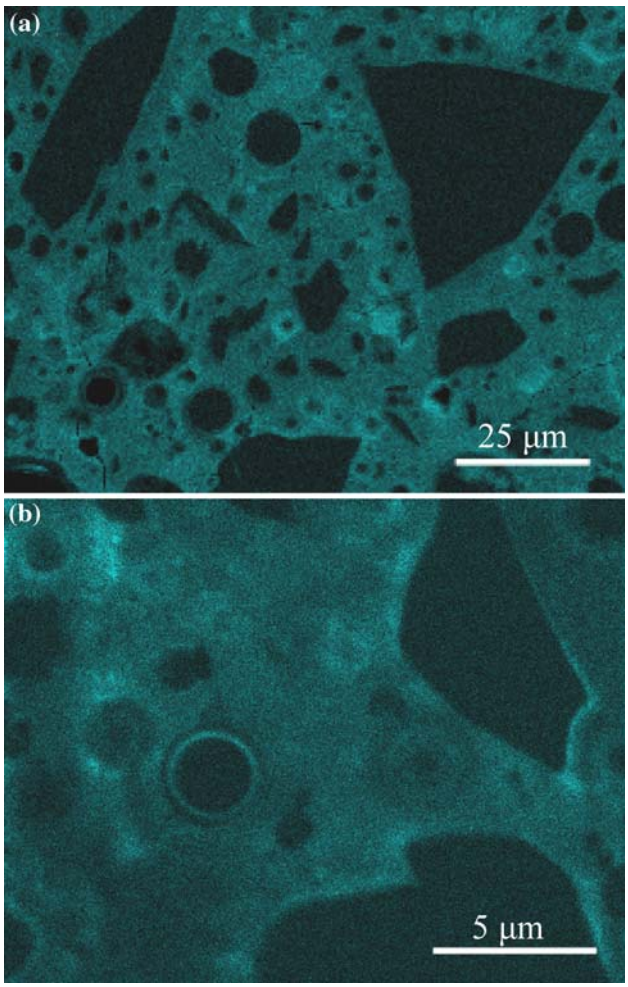

Fig. 6 Na K_α X-ray maps for blended GFA/GGBS-based IPC activated with sodium silicate solution (7 wt.% Na_2O, 7 wt.% SiO_2)

accelerating voltage of 5 kV) in blended GFA/GGBS pastes activated under the conditions studied here. In all cases, undissolved slag grains are visible and clearly contain more calcium than the gel. Within the gel, however, calcium distribution is relatively uniform. The behavior of calcium within the IPC binder is quite critical to the strength development rate of IPC, as the availability of calcium appears to lead to the development of high early strength. However, the exact mechanism by which this takes place—either via discrete calcium silicate hydrate formation, or by the formation of transient phases, or simply by enhancing aluminosilicate gel formation by acting as a charge-balancer—is not well understood.

The absence of a discrete calcium silicate hydrate (C–S–H) phase is potentially significant, and has consequences for the durability of IPC produced from blends of fly ash and GGBS [8]. The presence of discrete macroscopic phases, as observed in investigations of metakaolin-slag IPC [37–39], would result in phases of different properties, for instance resistance to acid or permeability. These could create paths with less resistance to degradation and thus reduce the durability of the products formed. The present work shows that these are not a feature of IPC synthesized from fly ash and GGBS. It is likely that such discrete phases result from inadequate mixing of raw materials, as discussed in detail elsewhere [8]. It should also be noted that inhomogeneous calcium distribution at a scale below the resolution of the SEM/EDX technique used here, i.e., a few hundred nanometers, cannot be ruled out on the basis of the evidence presented; further study using alternative experimental tools is required to provide this information in a definitive way.

Part of the difficulty in determining the distribution of calcium between different phases in IPC is the complexity introduced by the presence of slag, as significant differences are acknowledged to exist between fly ash-based IPC and alkali-activated slags [40]. Fly ash-based IPC is generally considered to have aluminum and silicon in a

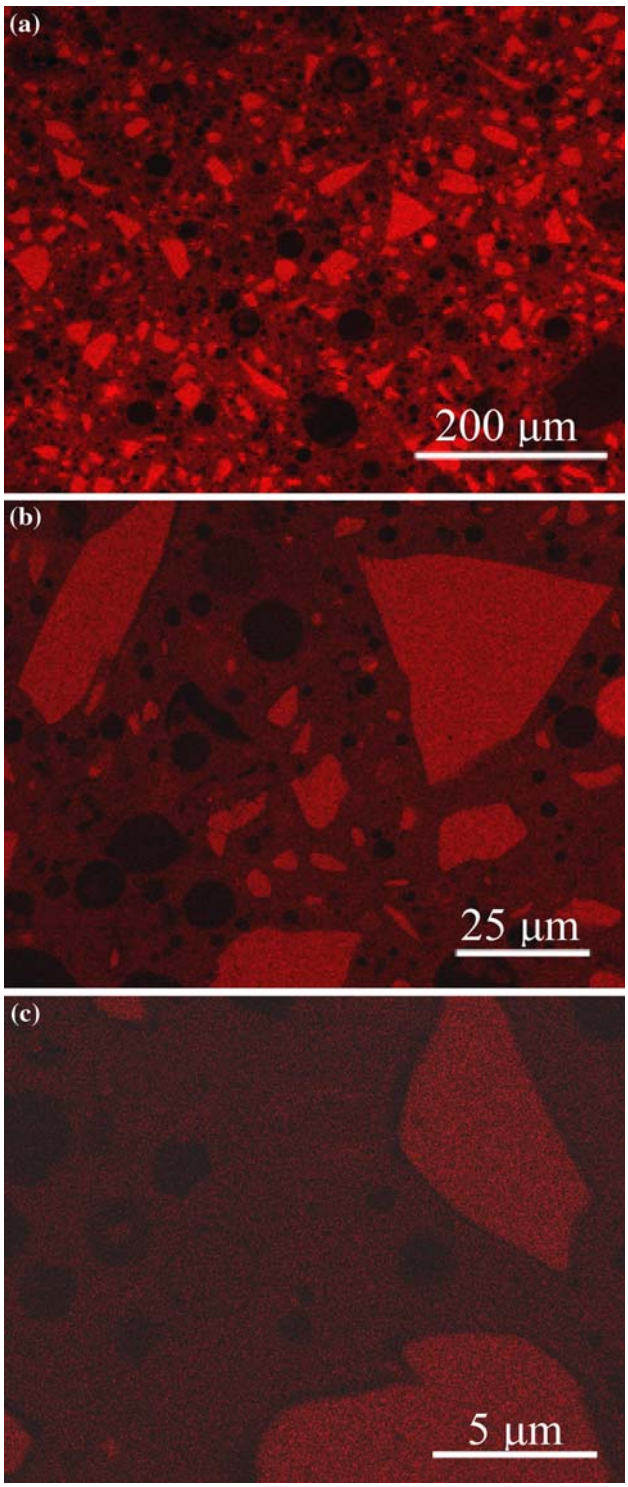

Fig. 7 Calcium K_α X-ray maps of a 1:1 GFA/GGBS IPC paste at various magnifications. Depletion of calcium around the rim of GGBS grains is apparent. Segregation into calcium-rich and calcium-deficient regions is not observed

three-dimensional network, with the majority of tetrahedral silicon or aluminum atoms bonded through oxygen atoms to four other tetrahedral centers [3]. Some nuclear

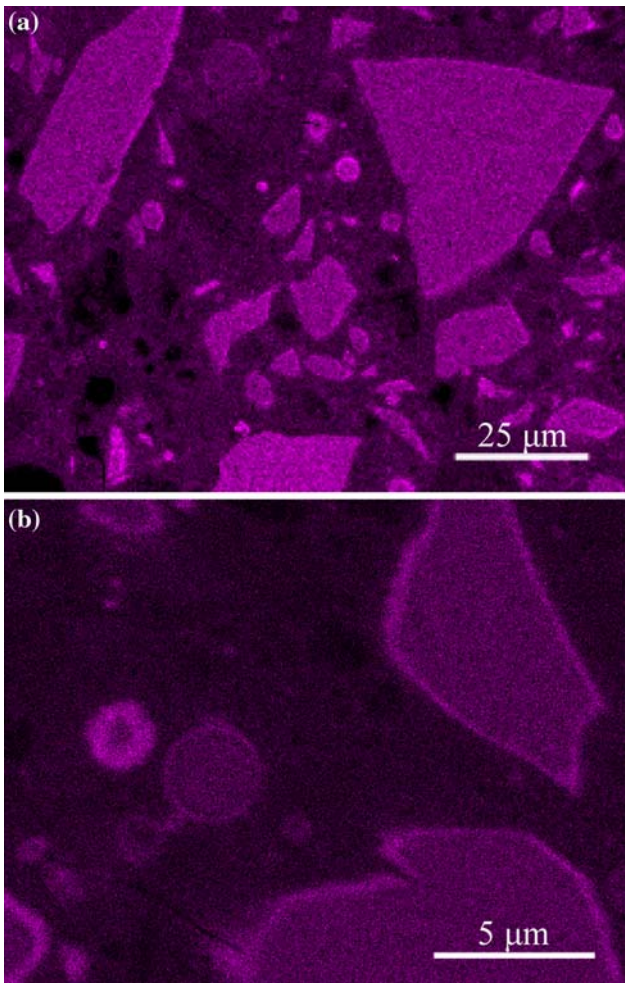

Fig. 8 Magnesium K_α X-ray maps for a blended (1:1) GFA/GGBS-based IPC activated with sodium silicate solution (7 wt.% Na_2O, 7 wt%. SiO_2)

magnetic resonance (NMR) evidence for this structure type has also been provided for blended fly ash/GGBS pastes by Allahverdi and Škvára [41]. The product of GGBS activated under the same conditions is calcium silicate hydrate [42], consisting primarily of linear chains of Si–O–Si, as shown by NMR spectroscopy [42, 43]. Although formed under the same activating conditions, the two structures proposed would seem to be incompatible; the exact nature of blended fly ash/GGBS-based IPC remains quite unclear.

Magnesium may be present in fly ash and/or GGBS; it is usually a more significant component of the latter due to the addition of dolomite to iron blast furnaces to produce slag. The fly ash used here is 1.35 wt.% MgO, while the slag is 6.02 wt.% MgO [1]. Figure 8 shows that some fly ash particles contain very little Mg while others are relatively richer; the Mg distribution within GGBS particles is uniform throughout the particle cores. However, enrichment of magnesium around the rims of GGBS grains is apparent in high magnification images. This coincides with

depletion of calcium and silicon, but not aluminum, in these regions (see Figs. 4, 5, and 7). As discussed in Part 1 [1], it remains unclear whether this is due to formation of a magnesium-rich hydrate such as hydrotalcite on the surface of slag grains or the presence of an alkali-insoluble magnesium-containing phase within the GGBS glass. However, in either case, it is clear that the magnesium remains in these regions rather than becoming distributed throughout the gel binder phase. This demonstrates a significant difference between the disposition of magnesium and calcium in IPC; even without the calcium forming macroscopically segregated C–S–H phases, there are marked differences in chemistry within the group of alkaline earth metals with regard to IPC formation.

Iron remains highly localized within unreacted fly ash particles in IPC pastes, as shown in Fig. 9. This agrees well with the low availability of iron as discussed in Part 1 [1]. It appears unlikely that iron plays a significant part in the actual formation of IPC gel. However, sorption of various system components onto iron-containing particles may have a significant influence on the chemistry of IPC synthesis; for example, its role in arsenic immobilization is observed to be significant, but the exact mechanisms taking governing this role are not yet completely clear [20]. It should also be noted that Yong et al. [44] have observed chemical bonding via T–O–Fe (T: tetrahedral matrix component, either Si or Al) linkages when metakaolin-based IPC was brought into contact with a steel surface; similar bonding to the oxide phases in remnant fly ash particles may be possible, but requires analytical tools other than electron microscopy to be assessed in detail.

Like magnesium, sulfur may be present in either fly ash or GGBS. The fate of sulfur in IPC has received little attention; it is apparent from Fig. 10 that GGBS contains marginally more sulfur than the gel, and those regions of high sulfur concentration exist. Sulfur may be responsible

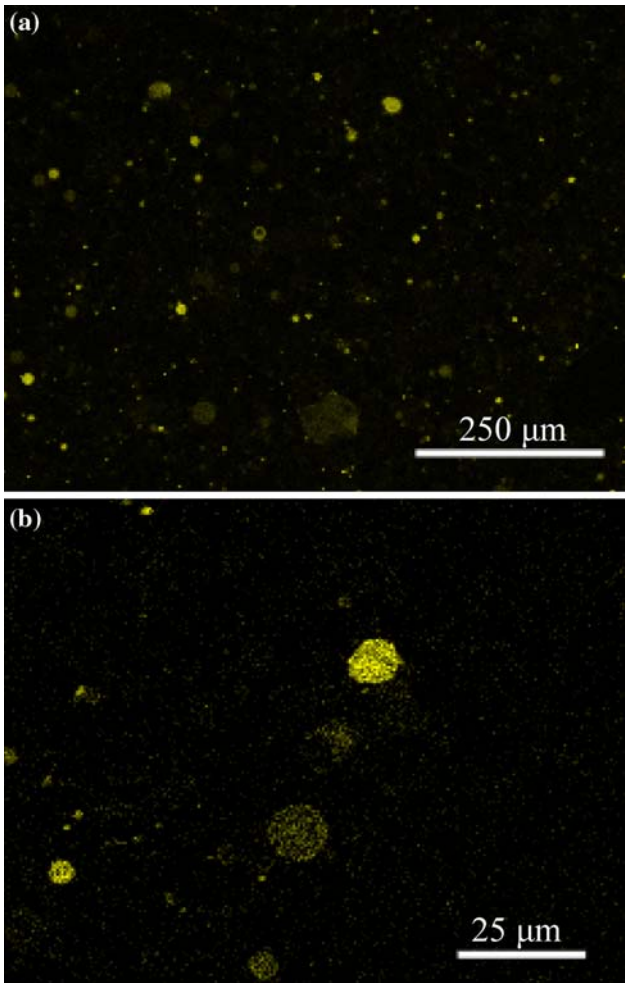

Fig. 9 Iron K_α X-ray maps for a blended (1:1) GFA/GGBS-based IPC activated with sodium silicate solution (7 wt.% Na_2O, 7 wt.% SiO_2)

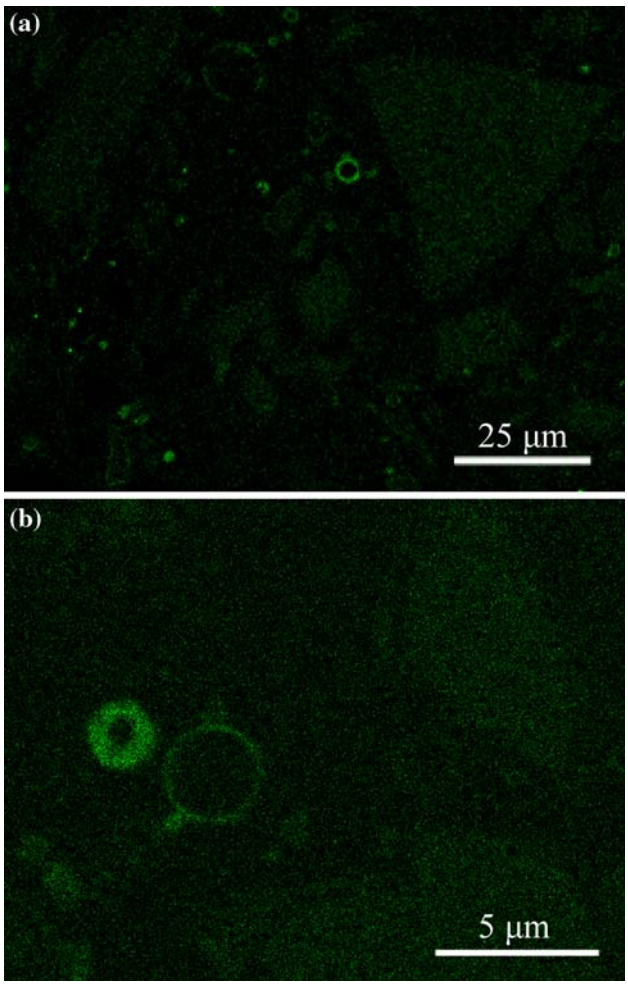

Fig. 10 Sulfur K_α X-ray maps for blended (1:1) GFA/GGBS-based IPC activated with sodium silicate solution (7 wt.% Na_2O, 7 wt.% SiO_2)

for the dark green color of many IPC samples which incorporate GGBS [45]. If so, control or elimination of sulfur, or control of its chemistry, may be important for obtaining light-colored products. This is highly desirable in many construction applications; certainly, most end users prefer their construction materials to be environmentally (figuratively) 'green' rather than literally green in color. The reaction proposed by Slavík et al. [45] for the generation of the green color, i.e., the entrapment of S_3^- radicals within a sodalite cage structure, may also provide some insight into the structure of the reaction products formed within the binder phase and should be further investigated.

Conclusion

The gels present in inorganic polymer cements synthesized with and without dissolved silica in the activating solution were examined, and the differences used to improve the understanding of the effect of silica solutions on IPC gel formation. The mechanistic distinction between silicate-activated and hydroxide-activated IPC formation is attributed to the differences in gel precipitation sites, with the hydroxide-activated gel forming predominantly on fly ash particle surfaces rather than by polymerization in the bulk region. The hypothesis developed correlates well with published results for strength and the degree of activation of fly ash with solutions of varying silicate content.

The distribution of elements in reacted IPC was also examined. It was found that the formation of discrete calcium-rich and calcium-deficient phases was not observed on the SEM length scale, meaning that if the gel is separated into such phases; this takes place at the nanometer level. This is important in terms of the durability of the IPC binder, as the differences in resistance to chemical attack between aluminosilicate and calcium silicate gels are believed to be significant. Silicon and aluminum are released in significant quantities by the dissolution of fly ash and slag particles, to form the IPC binder along with sodium supplied by the activating solution. Iron does not appear to move very far from its original position within fly ash particles. It is clear that much remains to be learned about the chemistry and microstructure of IPC. In particular, the fate of calcium at the atomic level needs to better understood, particularly given the importance of slag in producing economic and practical IPC.

Acknowledgements Partial financial support for this work was provided by the Australian Research Council (ARC), through Discovery Project grants awarded to J.S.J. van Deventer and through the Particulate Fluids Processing Centre, a Special Research Centre of the ARC.

References

1. Lloyd RR, Provis JL, van Deventer JSJ (2009) J Mater Sci, in press (Part 1 of this series). doi:10.1007/s10853-008-3077-0
2. Provis JL, van Deventer JSJ (2007) Chem Eng Sci 62:2318
3. Duxson P, Fernández-Jiménez A, Provis JL, Lukey GC, Palomo A, van Deventer JSJ (2007) J Mater Sci 42:2917. doi:10.1007/s10853-006-0637-z
4. Duxson P, Provis JL, Lukey GC, van Deventer JSJ (2007) Cem Concr Res 37:1590
5. Steveson M, Sagoe-Crentsil K (2005) J Mater Sci 40:4247. doi:10.1007/s10853-005-2794-x
6. Sindhunata, van Deventer JSJ, Lukey GC, Xu H (2006) Ind Eng Chem Res 45:3559
7. Rees CA, Provis JL, Lukey GC, van Deventer JSJ (2007) Langmuir 23:8170
8. Lloyd RR (2008) Ph.D. thesis, University of Melbourne, Australia
9. Richardson IG, Groves GW (1992) J Mater Sci 27:6204. doi:10.1007/BF01133772
10. Richardson IG (1999) Cem Concr Res 29:1131
11. Duxson P, Lukey GC, Separovic F, van Deventer JSJ (2005) Ind Eng Chem Res 44:832
12. Provis JL, van Deventer JSJ (2007) Chem Eng Sci 62:2309
13. Rees CA, Provis JL, Lukey GC, van Deventer JSJ (2007) Langmuir 23:9076
14. Bell JL, Sarin P, Provis JL, Haggerty RP, Driemeyer PE, Chupas PJ, van Deventer JSJ, Kriven WM (2008) Chem Mater 20:4768
15. Provis JL, Duxson P, Lukey GC, van Deventer JSJ (2005) Chem Mater 17:2976
16. Duxson P, Provis JL, Lukey GC, Mallicoat SW, Kriven WM, van Deventer JSJ (2005) Colloids Surf A 269:47
17. Fernández-Jiménez A, Palomo A, Criado M (2005) Cem Concr Res 35:1204
18. Kerch HM, Gerhardt RA, Grazul JL (1990) J Am Ceram Soc 73:2228
19. Fernández-Jiménez A, García-Lodeiro I, Palomo A (2007) J Mater Sci 42:3055. doi:10.1007/s10853-006-0584-8
20. Fernández-Jiménez A, Lachowski EE, Palomo A, Macphee DE (2004) Cem Concr Compos 26:1001
21. Criado M, Fernández-Jiménez A, de la Torre AG, Aranda MAG, Palomo A (2007) Cem Concr Res 37:671
22. Kinrade SD, Swaddle TW (1988) Inorg Chem 27:4253
23. Ray NH, Plaisted RJ (1983) J Chem Soc Dalton Trans 475
24. Phair JW, van Deventer JSJ (2002) Int J Miner Proc 66:121
25. Provis JL, Duxson P, Lukey GC, Separovic F, Kriven WM, van Deventer JSJ (2005) Ind Eng Chem Res 44:8899
26. Swaddle TW (2001) Coord Chem Rev 219–221:665
27. North MR, Swaddle TW (2000) Inorg Chem 39:2661
28. Knight CTG (1990) Zeolites 10:140
29. Cundy CS, Cox PA (2005) Micropor Mesopor Mater 82:1
30. Knight CTG, Wang J, Kinrade SD (2006) Phys Chem Chem Phys 8:3099
31. Lee WKW, van Deventer JSJ (2003) Langmuir 19:8726
32. Rees CA, Provis JL, Lukey GC, van Deventer JSJ (2008) Colloids Surf A 318:97
33. Lee WKW, van Deventer JSJ (2002) Colloids Surf A 211:49
34. Provis JL, Lukey GC, Van Deventer JSJ (2005) Chem Mater 17:3075
35. Rowles M, O'Connor B (2003) J Mater Chem 13:1161
36. Blackford MG, Hanna JV, Pike KJ, Vance ER, Perera DS (2007) J Am Ceram Soc 90:1193
37. Yip CK, Lukey GC, van Deventer JSJ (2005) Cem Concr Res 35:1688

38. Yip CK, van Deventer JSJ (2003) J Mater Sci 38:3851. doi:10.1023/A:1025904905176
39. Buchwald A, Hilbig H, Kaps C (2007) J Mater Sci 42:3024. doi:10.1007/s10853-006-0525-6
40. Shi C, Krivenko PV, Roy DM (2006) Alkali-activated cements and concretes. Taylor & Francis, Abingdon
41. Allahverdi A, Škvára F (2001) Ceram-Silik 45:143
42. Brough AR, Atkinson A (2002) Cem Concr Res 32:865
43. Cong X, Kirkpatrick RJ (1996) Adv Cem Based Mater 3:144
44. Yong SL, Feng DW, Lukey GC, van Deventer JSJ (2007) Colloids Surf A 302:411
45. Slavík R, Bednařík V, Vondruška M, Skoba O, Hanzlíček T (2005) Chem Listy 99:s471